Journal of Power Sources 189 (2009) 1032–1043

Contents lists available at ScienceDirect

Journal of Power Sources

journal homepage: www.elsevier.com/locate/jpowsour

Optimization of La_2O_3-containing diopside based glass-ceramic sealants for fuel cell applications

Ashutosh Goel[a,b], Dilshat U. Tulyaganov[a,c], Vladislav V. Kharton[a], Aleksey A. Yaremchenko[a], Sten Eriksson[b], José M.F. Ferreira[a,*]

[a] Department of Ceramics and Glass Engineering, University of Aveiro, CICECO, 3810-193 Aveiro, Portugal
[b] Environmental Inorganic Chemistry, Chalmers University of Technology, 412 96 Gothenburg, Sweden
[c] State Committee of Geology and Mineral Resources, Centre of remote sensing and GIS technologies, 11-A, Shevchenko str., 100060 Tashkent, Uzbekistan

ARTICLE INFO

Article history:
Received 11 October 2008
Received in revised form 9 December 2008
Accepted 7 January 2009
Available online 19 January 2009

Keywords:
Glass-ceramic sealant
Solid oxide fuel cell (SOFC)
Coefficient of thermal expansion (CTE)
Interaction
Interconnect

ABSTRACT

We report on the optimization of La_2O_3-containing diopside based glass-ceramics (GCs) for sealant applications in solid oxide fuel cells (SOFC). Seven glass compositions were prepared by modifying the parent glass composition, $Ca_{0.8}Ba_{0.1}MgAl_{0.1}La_{0.1}Si_{1.9}O_6$. First five glasses were prepared by the addition of different amounts of B_2O_3 in a systematic manner (i.e. 2, 5, 10, 15, 20 wt.%) to the parent glass composition while the remaining two glasses were derived by substituting SrO for BaO in the glasses containing 2 wt.% and 5 wt.% B_2O_3. Structural and thermal behavior of the glasses was investigated by infrared spectroscopy (FTIR), density measurements, dilatometry and differential thermal analysis (DTA). Liquid–liquid amorphous phase separation was observed in B_2O_3-containing glasses. Sintering and crystallization behavior, microstructure, and properties of the GCs were investigated under different heat treatment conditions (800 and 850 °C; 1–300 h). The GCs with ≥5 wt.% B_2O_3 showed an abnormal thermal expansion behavior above 600 °C. The chemical interaction behavior of the glasses with SOFC electrolyte and metallic interconnects, has been investigated in air atmosphere at SOFC operating temperature. Thermal shock resistance and gas-tightness of GC sealants in contact with 8YSZ was evaluated in air and water. The total electrical resistance of a model cell comprising Crofer 22 APU and 8YSZ plates joined by a GC sealant has been examined by the impedance spectroscopy. Good matching of thermal expansion coefficients (CTE) and strong, but not reactive, adhesion to electrolyte and interconnect, in conjunction with a low level of electrical conductivity, indicate that the investigated GCs are suitable candidates for further experimentation as SOFC sealants.

1. Introduction

Glass-ceramic (GC) materials are ideal candidates for sealing and coating applications where compatible thermal expansions are essential. Most recently, there has been a dramatic revival of interest in both glass- and GC-to-metal seals, particularly for new applications including sealants in SOFC [1,2]. Substantial work is in progress in this area, aimed at improving the performance of these sealants under extreme operating conditions of current fuel cell designs, which involve both high temperatures and highly corrosive environments. Most of the GC based sealants proposed so far are alkaline earth aluminosilicate based; borate based or borosilicate GCs [1,3,4]. However, every material has some advantages which are coupled along with some drawbacks. Therefore, still there is a need to fill in this lacuna by developing a suitable sealing material for SOFC technology.

Recently, we proposed a La_2O_3-containing diopside based GC seal for SOFC with very low amounts of BaO [5]. The choice of diopside based GCs for the application of sealants in SOFC was based on the attractive features exhibited by their chemical composition, as summarized in Table 1 [6]. The GC seal demonstrated a sufficiently high CTE ($\sim 10 \times 10^{-6}\,K^{-1}$) after heat treatment at 900 °C for 300 h in air along with the absence of detrimental monocelsian phase. High electrical resistance and activation energy of total conductivity = 172 kJ mol^{-1}, in combination with strong adhesion, and high chemical stability with Crofer22 APU alloy and 8YSZ were its other attributes. However, still there is need to reduce the glass transition temperature, T_g and softening temperature, T_s of the residual glassy phase in order to avoid the formation of cracks due to stress which appear during the cooling of the SOFC stack. Also, an increase in the CTE of the GC is required so that it can successfully work at intermediate temperatures and can adhere effectively to the components, especially metallic interconnects of SOFCs.

The decrease in viscosity and crystallization tendency of the silicate glasses (both of which are favorable properties) with the addition of B_2O_3 is well known. According to Sohn et al. [7],

* Corresponding author. Tel.: +351 234 370242; fax: +351 234 370204.
E-mail address: jmf@ua.pt (J.M.F. Ferreira).

0378-7753/$ – see front matter © 2009 Elsevier B.V. All rights reserved.
doi:10.1016/j.jpowsour.2009.01.013

Table 1
Common compositional modifiers for silicate based GCs.

Modifier	Function
Al_2O_3	Allows control over viscosity through the rate of crystallization
B_2O_3	Reduces T_g, T_s, and viscosity and improves wetting
La_2O_3	Used as a viscosity modifier and long-term CTE stabilizer
BaO	Reduces T_g and T_s, and raises CTE in the GC
CaO	Reduces T_g and T_s, and raises CTE in the GC
MgO	Reduces T_g and T_s, and raises CTE in the GC; improves surface adhesion
SrO	Stimulates crystallization
NiO	Improves adhesion

B_2O_3/SiO_2 ratio plays an important role in tailoring the properties of the GC sealants as the CTE of the glasses has been observed to increase with increase in B_2O_3/SiO_2 ratio. However, the disadvantage of adding B_2O_3 is that, at operating temperatures, B_2O_3 forms volatile compounds with water vapor leading to seal degradation [8]. Therefore, high amount of B_2O_3 in the sealants is not seen with alacrity. Most sealing glasses studied to date are of the borosilicate type [1].

Moreover, it has been widely accepted that the BaO reacts with the Cr from the metallic interconnect under oxidizing environment so as to produce $BaCrO_4$ which is highly detrimental for the SOFC stack [1]. Significant content of BaO may also promote interaction with water vapor, leading to slow sealant degradation under SOFC operating conditions. Thus, in order to avoid such a condition, replacement of BaO by SrO has been attempted, in the present study, as an alternative, and various properties of the as produced glasses and GCs have been investigated. Previously, Ley et al. [9] studied the glass and GC system of $SrO–Al_2O_3–La_2O_3–SiO_2–B_2O_3$. The CTE values of the as-made materials were in the range of $8–13 \times 10^{-6}\,K^{-1}$, while the long-term stability was not reported. Recently, Brochu et al. [10] compared the performance of the BaO- and SrO-based borate glass-composites for sealing materials in SOFCs and reported the formation of low CTE crystalline phase, $BaZrO_3$, on interaction with 8YSZ, for BaO containing glass-composites. However, in case of SrO-based glass-composites, formation of strontium zirconates was observed, which has CTE similar to 8YSZ. Kumar et al. [11] studied the MgO/SrO-based borosilicate glasses and observed that SrO containing glasses had higher CTE in comparison to MgO-based glasses. In a recent study, Mahapatra et al. [12] investigated the thermophysical properties and devitrification behavior of the glasses in the system $(25-X)SrO–20La_2O_3–(7+X)Al_2O_3–40B_2O_3–8SiO_2$ (mol%) (X = 0–10). However, as mentioned above, high boron seals proposed in earlier studies [9–12] are apt to eventually corrode under humidified hydrogen environments (common in fuel cell operation) over time. So, this also justifies the need to make this investigation.

Therefore, taking into consideration the previously reported results, a series of new glass compositions were prepared. In particular, an attempt has been made to tailor the properties of the La_2O_3-containing diopside based glasses and GCs [5] by the addition of varying amounts of B_2O_3 to the parent glass ($Ca_{0.8}Ba_{0.1}MgAl_{0.1}La_{0.1}Si_{1.9}O_6$) in a systematic manner. The first five compositions were derived from the glass composition $Ca_{0.8}Ba_{0.1}MgAl_{0.1}\ La_{0.1}Si_{1.9}O_6$, (labeled as 7A), which was investigated in our previous study [5], by the addition of different amounts of B_2O_3 to it varying between 2 and 20 wt.%. To be consistent with our previous study, these compositions are labeled as 7-2B, 7-5B, 7-10B, 7-15B and 7-20B, respectively, where, 2B, 5B, 10B, 15B and 20B designate the amount of B_2O_3 incorporated into the parent glass. The remaining two compositions were derived from 7-2B and 7-5B by replacement of Ba for Sr and are labeled as 7(Sr)-2B and 7(Sr)-5B. Table 2 presents the details of the seven compositions investigated in the present work. The parent glass composition, 7A, is presented in Table 2 as a reference and some previous and new results obtained from the investigations on this composition are also presented and discussed, along with those obtained from its derivative compositions, in the present manuscript. Furthermore, a detailed investigation has been made on the as produced glasses and GCs, in order to optimize their properties suitable for sealants in SOFC.

2. Experimental

Powders of technical grade SiO_2 (purity >99.5%) and $CaCO_3$ (>99.5%), and of reactive grade H_3BO_3, Al_2O_3, $MgCO_3$, $BaCO_3$, La_2O_3, Cr_2O_3 and NiO were used. Homogeneous mixtures of batches (∼100 g), according to Table 2, obtained by ball milling, were preheated at 900 °C for 1 h for decarbonization and then melted in Pt crucibles at 1550 °C for 1 h, in air.

Glasses in bulk form were produced by pouring the melts on preheated bronze moulds followed by annealing at 550 °C for 1 h. The samples of the glass-powder compacts were produced from glass frits, which were obtained by quenching of glass melts in cold water. The frits were dried and then milled in a high-speed agate mill resulting in fine glass powders with mean particle sizes of 10–15 μm (determined by light scattering technique; Coulter LS 230, Beckman Coulter, Fullerton CA; Fraunhofer optical model). Circular disc shaped pellets with Ø 20 mm and thickness ∼3 mm were prepared from glass powders by uniaxial pressing (80 MPa). The pellets were sintered under non-isothermal conditions for 1 h at 800 and 850 °C, respectively. A slow heating rate of 2 K min^{-1} was maintained in order to prevent deformation of the samples. Further, pellets already sintered at 850 °C, were heat treated under isothermal conditions at 800 °C for 300 h. In order to examine the possibility of existence of liquid–liquid amorphous phase separation, glasses in bulk form were heat treated at 700 °C for 1 h at heating rate of 5 K min^{-1}.

Infrared spectra for the glass powders were obtained using an Infrared Fourier spectrometer (FT-IR, model Mattson Galaxy S-7000, USA). For this purpose, each sample powder was mixed with KBr in the proportion of 1/150 (by weight) and pressed into a pellet using a hand press.

Dilatometry measurements were done on prismatic samples with a cross section of 4 mm × 5 mm (Bahr Thermo Analyze DIL 801 L, Hüllhorst, Germany; heating rate 5 K min^{-1}). A minimum of 3 samples for each composition were analyzed. Glass transition temperature (T_g), softening point (T_s) and CTE were obtained in the permissible limits of experimental errors. Differential thermal analysis of fine powders was carried out in air (DTA-TG, Setaram Labsys, Setaram Instrumentation, Caluire, France) at heating rate (β) of 5 K min^{-1}.

The linear shrinkage during sintering was calculated from the difference of the diameter between the green and the sintered pellets. Archimedes' method (i.e. immersion in diethyl phthalate) was employed to measure the apparent density (ρ) of the bulk annealed glasses and sintered GCs. The mean values and the standard deviations (SD) presented for linear shrinkage and density have been obtained from (at least) 10 different samples.

To investigate the adhesion and chemical interaction of the glasses with SOFC components, wetting experiments between glass (powder)-SOFC electrolyte, 8YSZ (zirconia stabilized by 8 mol% yttria; Tosoh, Japan) and glass (powder)-metallic interconnect were carried out under different conditions. Two different metallic interconnect materials, namely, Crofer22 APU (Thyssen Krupp, VDM, Werdohl, Germany) and Sanergy HT (Sandvik AB, Sandviken, Sweden) were employed for wetting and interaction experiments with the glasses. Table 3 [13,14] presents the composition of the two interconnect materials. The glass powders were deposited on electrolyte and interconnect by slurry coating. Joined interconnect-

Table 2
Batch compositions of the glasses.

Glass		MgO	CaO	BaO	SrO	SiO_2	Al_2O_3	La_2O_3	B_2O_3	NiO
7A	wt.%	16.90	18.82	6.43	–	47.88	2.14	6.83	–	1
	mol%	25.43	20.35	2.54	–	48.32	1.27	1.27	–	0.81
	mol ratio	1	0.8	0.1	–	1.9	0.05	0.05	–	0.032
7-2B	wt.%	16.56	18.44	6.30	–	46.91	2.09	6.70	2	1
	mol%	24.98	19.99	2.50	–	47.47	1.25	1.25	1.75	0.81
	mol ratio	1	0.8	0.1	–	1.9	0.05	0.05	0.07	0.033
7-5B	wt.%	16.05	17.87	6.11	–	45.46	2.03	6.49	5	1
	mol%	24.31	19.45	2.43	–	46.18	1.22	1.22	4.38	0.82
	mol ratio	1	0.8	0.1	–	1.9	0.05	0.05	0.18	0.034
7-10B	wt.%	15.20	16.92	5.78	–	43.04	1.92	6.14	10	1
	mol%	23.17	18.53	2.32	–	44.02	1.16	1.16	8.82	0.82
	mol ratio	1	0.8	0.1	–	1.9	0.05	0.05	0.38	0.036
7-15B	wt.%	14.34	15.97	5.46	–	40.62	1.81	5.80	15	1
	mol%	22.01	17.61	2.20	–	41.82	1.10	1.10	13.33	0.83
	mol ratio	1	0.8	0.1	–	1.9	0.05	0.05	0.61	0.038
7-20B	wt.%	13.49	15.01	5.13	–	38.20	1.71	5.45	20	1
	mol%	20.84	16.67	2.08	–	39.60	1.04	1.04	17.89	0.83
	mol ratio	1	0.8	0.1	–	1.9	0.05	0.05	0.86	0.04
7(Sr)-2B	wt.%	16.92	18.83	–	4.35	47.92	2.14	6.84	2	1
	mol%	25	20	–	2.50	47.50	1.25	1.25	1.71	0.80
	mol ratio	1	0.8	–	0.1	1.9	0.05	0.05	0.07	0.032
7(Sr)-5B	wt.%	16.40	18.25	–	4.22	46.44	2.07	6.63	5	1
	mol%	24.33	19.47	–	2.43	46.24	1.22	1.22	4.30	0.80
	mol ratio	1	0.8	–	0.1	1.9	0.05	0.05	0.18	0.033

glass-electrolyte samples were obtained by sandwiching the glass coated YSZ wafer and the interconnect plate. Heat treatment was performed in a tubular furnace, without applying any dead load, in air atmosphere. The diffusion couples were heated to 850 °C with a relatively slow heating rate (2 K min^{-1}) and kept at that temperature for 1 h. Finally, the temperature was brought down to SOFC operating temperature (i.e. 800 °C) and maintained at this temperature for 300 h. Energy dispersive spectroscopy (EDS; Bruker Quantax, Germany) was employed to study the distribution of elements along the glass-interconnect diffusion couples.

The amorphous nature of the glasses and crystalline phases in the GCs were determined by X-ray diffraction (XRD) analysis (Rigaku Geigerflex D/Max, C Series, Tokyo, Japan; Cu Kα radiation; 2θ angle range 10–80°; step 0.02 ° s^{-1}). The phase transformations occurring in fine GC powders (already sintered at 850 °C for 1 h) over increasing temperature were monitored by *in situ* high temperature X-ray diffraction (HT-XRD) analysis (Philips, X'pert, The Netherlands, equipped with a Pt hot stage). The schedule of the hot stage was as follows: Heating up to 650 °C with a rate of 5 K min^{-1} and immediate collection of XRD data without any dwell, and then a similar ramp (5 K min^{-1}) and no dwell for obtaining the diffractograms at 700, 750 and 800 °C.

Microstructure observations were done on polished (mirror finishing) samples. The etching of glasses and GCs was done by immersion in 2 vol.% HF solution for different time durations (i.e. 5 s for glasses and 2 min GCs) while the unetched 8YSZ/GC/interconnect interfaces (cross-sectioned) were observed by field emission scanning electron microscopy (FE-SEM, Hitachi S-4100, Tokyo, Japan; 25 kV acceleration voltage, beam current 10 μA) under secondary electron mode.

The total conductivity was studied by the AC impedance spectroscopy (HP4284A precision LCR meter, 20 Hz–1 MHz, Agilent Technologies, Palo Alto, CA), using dense disk-shaped samples with porous Pt electrodes and Pt current collectors, in atmospheric air. In the course of impedance measurements, the magnitude of AC voltage was fixed at 1.00 V; the equilibration time after each temperature change was 2–4 h. The same method was used to test the total electrical resistance of a model cell comprising Crofer 22 APU and 8YSZ plates joined by the GC sealant, with Pt electrodes deposited onto the metal and zirconia plates.

In order to evaluate thermal shock resistance of the GC sealants in contact with stabilized zirconia electrolyte, a series of cells were made of 8YSZ by sealing dense ceramic tubes onto the disks. Hermetic sealing was performed using powdered GCs, with final annealing at 1250 °C for 0.5 h. Then each pseudo-cell was heated in the furnace up to 800 °C, kept at this temperature for 0.5 h, and quenched in air or in water. After subsequent checking of the gas-tightness, each cell was rapidly heated again, and the quenching cycle was repeated. The YSZ pseudo-cells were successfully tested in 15 air-quenching cycles.

Table 3
Chemical composition of metallic interconnect (wt.%).

	Crofer22 APU										
	Cr	Fe	C	Mn	Si	Cu	Al	S	P	Ti	La
Min.	20.0	Bal.	–	0.30	–	–	–	–	–	0.03	0.04
Max.	24.0		0.03	0.80	0.50	0.50	0.50	0.020	0.050	0.20	0.20

Sanergy HT						
C (max.)	Si (max.)	Mn (max.)	Cr	Mo	Nb	Other
0.05	0.30	0.50	22	1.0	0.75	Ti

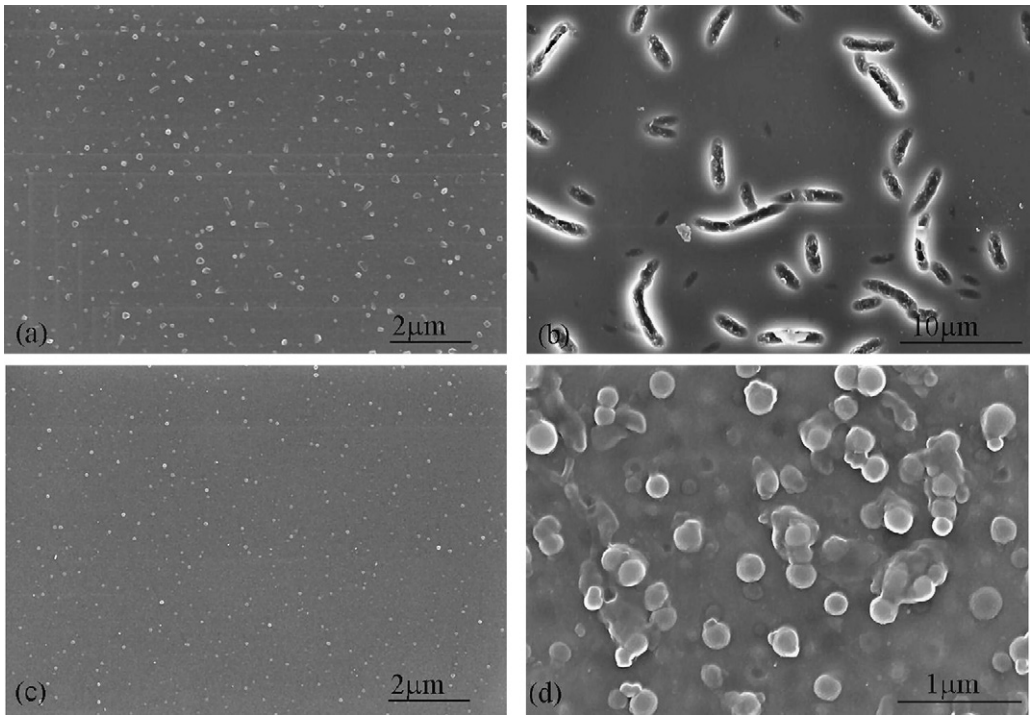

Fig. 1. SEM images of glasses (a) 7-2B, (b) 7-5B, (c) 7-10B after heat treatment at 700 °C for 1 h, respectively and (d) 7-20B (as casted and annealed at 550 °C for 1 h).

3. Results and discussion

3.1. Characterization of the glasses

3.1.1. Casting ability and microstructural features

The compositions containing 2, 5 and 10 wt.% B_2O_3 (Table 2) were prone to easy casting after 1 h of melting (at 1550 °C), resulting in homogenous transparent glasses with brown color. A similar brown colored glass but with a dull appearance was obtained for the composition containing 15 wt.% B_2O_3 (7-15B). The origin of this brown coloration in the glasses is due to the presence of nickel in five-coordination, in trigonal bipyramids [15]. For composition containing 20 wt.% B_2O_3 (7-20B), we obtained a light brown colored opaque glass. The amorphous nature of as cast and annealed glasses was confirmed by XRD analysis.

The SEM images of the bulk glasses (heated at 700 °C for 1 h) (Fig. 1a–c) showed the existence of phase separation in B_2O_3-containing glasses. However, the type of phase separation seems to change with the variation in boron content in the glasses. The glasses with 2 wt.% B_2O_3 (Fig. 1a) showed nucleated droplet phase separation while spinodal decomposition was observed with addition of 5 wt.% B_2O_3 (7-5B) (Fig. 1b). Further, with an increasing B_2O_3 in the glasses, nucleated droplet phase separation was observed (Fig. 1c). A large number of homogeneously distributed round shaped droplets of size 150–200 nm were observed in as cast and annealed glass 7-20B (Fig. 1d). Due to lack of transparency and strong tendency for phase separation, this particular composition was not considered for further investigation.

Along the series of the investigated compositions of Table 2, the properties values summarized in Table 4 reveal the following general features:

3.1.2. Density and molar volume

The experimental results showed that the addition of B_2O_3 led to a decrease in the density (ρ) of the glasses (Table 4). Since, density of a glass is an additive property and density of B_2O_3 is the lowest among all the constituents of the glasses ($\rho = 2.55\ g\,cm^{-3}$) except that of SiO_2 ($\rho = 2.53\ g\,cm^{-3}$), therefore, a decrease in density with increasing B_2O_3 contents is logical. SrO-containing glasses exhibit lower density than their BaO-containing counterparts because density of SrO ($\rho = 5.10\ g\,cm^{-3}$) is lower in comparison to that of BaO ($\rho = 5.72\ g\,cm^{-3}$).

The molar volume (V_m) and excess molar volume (V_e) were calculated using the apparent density data for the bulk glasses using the relations that have already been reported in our previous work [5]. The highest values of V_m and V_e were obtained for glass 7-15B and the lowest for glass 7-2B. The values of V_m and V_e for the glasses under investigation are higher than the parent glass

Table 4
Properties of the glasses.

	7A	7-2B	7-5B	7-10B	7-15B	7(Sr)-2B	7(Sr)-5B
ρ ($g\,cm^{-3}$)	3.08 ± 0.001	3.06 ± 0.005	3.02 ± 0.001	2.96 ± 0.004	2.91 ± 0.003	3.02 ± 0.005	2.98 ± 0.003
V_m ($cm^3\,mol^{-1}$)	19.71 ± 0.012	19.88 ± 0.035	20.22 ± 0.006	20.51 ± 0.023	21.24 ± 0.021	19.74 ± 0.035	20.08 ± 0.023
V_e ($cm^3\,mol^{-1}$)	0.24 ± 0.012	0.28 ± 0.035	0.41 ± 0.006	0.36 ± 0.023	0.74 ± 0.021	0.30 ± 0.035	0.44 ± 0.023
T_g (±2) (°C)	685	580	575	530	490	533	545
T_s (±5) (°C)	716	710	698	680	665	665	672
(CTE ± 0.1) × $10^6\ K^{-1}$ (200–500 °C)	8.69	7.91	7.79	7.56	7.50	7.99	8.08
T_p (°C)	912	896	874	859	855	891	871

T_g, T_s, CTE and T_p values are for $\beta = 5\ °C\,min^{-1}$.

composition, 7A (Table 4). Also, unlikely to the results obtained in our previous study [5], V_m increased with the decrease in the density of the BaO-containing glasses, in the present investigation. V_m for SrO-containing glasses is lower while V_e is higher than their BaO-containing analogs (7-2B and 7-5B), respectively. The incorporation of B_2O_3 increases the covalent nature of the glasses. Owing to the formation of directional bonds in the structural skeleton of the glass with the increasing B_2O_3 contents, molar volume and excess volume increases [16].

3.1.3. Dilatometry

In general, T_g, T_s and CTE decreased considerably with introduction of B_2O_3 in the parent glass composition, 7A (Table 4). This trend in variation of T_g and T_s may be explained on the basis of two competing mechanisms: (a) B_2O_3/SiO_2 ratio in the glasses and (b) conversion of three-coordinated boron (B_3) to four-coordinated boron (B_4) (as will also be discussed in Section 3.1.4). The decrease in T_g with increase in B_2O_3 content may be attributed to the increasing B_2O_3/SiO_2 ratio in the glasses. B_2O_3/SiO_2 ratio has been reported to have a significant effect on the T_g and T_s of the glasses [8,17]. The activation energies of viscous flow for SiO_2 and B_2O_3 are 710 kJ mol^{-1} (1100–1400 °C) and 347–50 kJ mol^{-1} (26–1300 °C), respectively [18]. Since, T_g of a glass is a function of its viscosity, therefore, decreasing viscosity implies a decrease in T_g. Even though, conversion of B_3 to B_4 must have occurred with increasing B_2O_3 content, however, it seems that until glass 7-15B, the concentration of B_3 dominated. Further experimental studies related to the quantification of B_3 and B_4 structural units in these glasses are required to obtain a better insight on the structure of these glasses. The T_g and T_s for SrO-containing glasses were lower in comparison to their BaO-containing analogs (Table 4) due to the decrease in polymerization of silicate glass network, as discussed in Section 3.1.4.

The CTE value decreased with increasing B_2O_3 contents, while the CTE values for glasses 7(Sr)-2B and 7(Sr)-5B were higher in comparison to glasses 7-2B and 7-5B, respectively. According to Ojovan and Lee [19], addition of B_2O_3 up to 15 wt.% in a borosilicate glass decreases the CTE of the glass. The change in the CTE of the glasses with variation of boron content and replacement of Sr for BaO has been explained with the help of FTIR analysis of the glasses in the Section 3.1.4. However, it should be noted that this anomalous thermal expansion of the glasses with change in B_2O_3 content should not be attributed to the existence of phase separation in these glasses [20]. Similar results have also been reported in glazes where lower amount of boron oxide prevents crazing in glazes, while addition of more than 15 wt.% B_2O_3 shows an opposite effect because the resilience of glazes decreases with high amount of B_2O_3. This behavior of B_2O_3 in glazes is termed as boracitis [21].

With respect to the development of a suitable GC sealant, optimization of T_g of the glass is a crucial step, as above T_g the mechanical properties of the glass change from brittle to elastic. However, the brittle nature of the glass below this temperature makes the seal vulnerable to cracking. Therefore, it is necessary to obtain the seal with low T_g and T_s. The T_g and T_s values obtained in the present investigation for glasses containing $\leq$10 wt.% B_2O_3 are appropriate for sealant application in SOFC.

3.1.4. FTIR analysis

The room temperature FTIR transmittance spectra of all the six investigated glasses are shown in Fig. 2. All spectra exhibit four broad transmittance bands in the region of 300–1500 cm^{-1}. This lack of sharp features is indicative of the general disorder in the silicate network mainly due to a wide distribution of Q_n (polymerization in the glass structure, where n denotes the number of bridging oxygens) units occurring in these glasses. The most intense bands lie in the 800–1300 cm^{-1} region, the next between

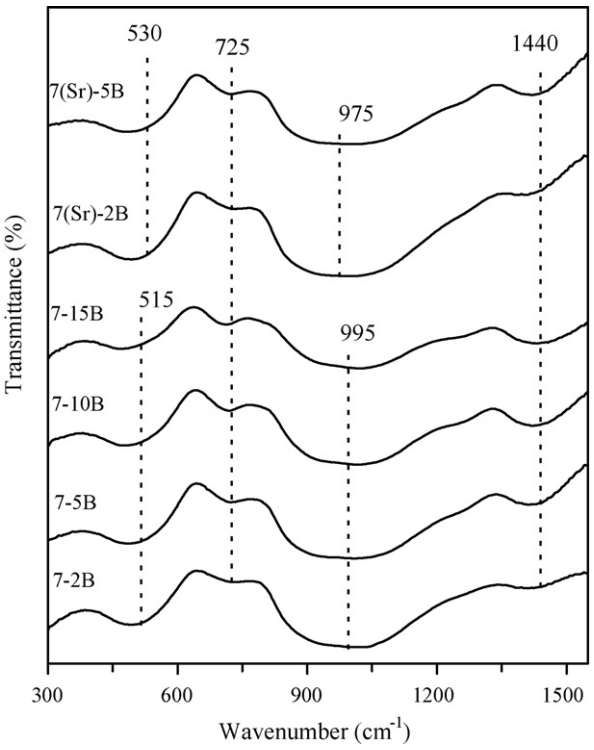

Fig. 2. FTIR spectra of the investigated glass powders.

300–600 cm^{-1} and 1350–1500 cm^{-1}, while the least intensive lies between 650 and 800 cm^{-1}. The broad bands in the 800–1300 cm^{-1} are assigned to the stretching vibrations of the SiO_4 tetrahedron with a different number of bridging oxygen atoms, while the bands in the 300–600 cm^{-1} region are due to bending vibrations of Si–O–Si and Si–O–Al linkages [22,23]. In the present study, the bands in 800–1300 cm^{-1} region were registered at considerably lower wave numbers than those observed for B_2O_3-free parent glass in our previous study [5]. Thus, it is evident that the introduction of B_2O_3 breaks up Q_3 units and favors the formation of Q_2 units. These results are in accordance with those of Ojovan and Lee [19], according to whom, the introduction of boron in the silicate glass leads to the breaking up of Q_3 units and the formation of Q_2, Q_4 and small amounts of Q_1 units. A slight shift towards lower wave numbers has been registered in the 800–1300 cm^{-1} band with the replacement of Ba by Sr. This suggests that the SrO-depolymerizes the silicate glass network in an efficient manner in comparison to BaO. The transmittance bands in the 650–800 cm^{-1} region are related to the stretching vibrations of the Al-O bonds with Al^{3+} ions in four-fold coordination [22]. Aluminum is known to create Q_3 bands at the expense of Q_2 and Q_4 units in the silicate glasses [23]. The transmittance band in the region 1350–500 cm^{-1} corresponds to B–O vibrations in [BO_3] triangle [24]. As is evident from Fig. 2, an increase in B_2O_3 content did not affect the silicate glass network. This may be due to the conversion of boron from B_3 to B_4 in the presence of alkaline earth ions. In a borosilicate glass, alkali or alkaline earth metals may associate either with silicon, creating non-bridging oxygen (NBO), or with boron, presumably converting a B_3 to B_4 and creating no NBOs in the process [25]. The bond between a bivalent ion and the centers of two boron-oxygen tetrahedrons is stronger than the bond between outside oxygens of silicon-oxygen tetrahedrons (as is also the case with alkali ions). Therefore, it can be presumed that alkaline earth ions prefer to be associated with the borate component. This increase in connectivity causes the CTE to decrease. This effect has also been observed in alkali-borosilicate glasses and was attributed to the commonly known 'boron anomaly' [25]. Since, the

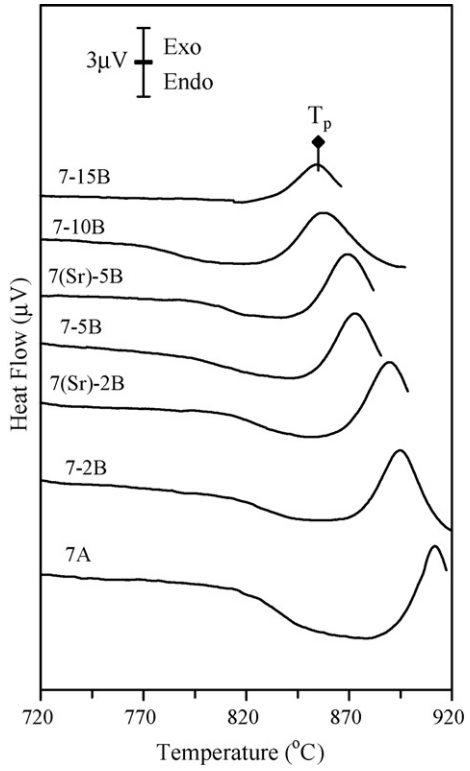

Fig. 3. Differential thermal analysis (DTA) of fine powders of the investigated glasses heated at a rate of 5 K min^{-1}.

IR band for [BO_4] tetrahedron (about 1000 cm^{-1}) overlaps with that of stretching vibrations of SiO_4, it could not therefore be observed in the present investigation. The results obtained from dilatometry and FTIR analysis show that the network structure of experimental boron containing glasses is complex, containing mostly silicon Q_n as well as boron B_3 and B_4 groups. Due to preferential association of alkaline earth ions with the borate component, conversion of boron from B_3 to B_4 occurs with increasing B_2O_3 content, causing the CTE to decrease. This interpretation supports the trends previously observed in borosilicate glasses [19]. Nevertheless, further experimentation including NMR measurements of the concentration Q_n silicate and borate units is required to better understand the structure of these multicomponent glasses and the composition-property trends observed in the present investigation. The above discussed results are in agreement with the results obtained from the calculations of V_m and V_e. No other band could be resolved in the spectra of the glasses.

3.1.5. Differential thermal analysis (DTA)

The DTA plots of fine powders with a heating rate of 5 K min^{-1}, shown in Fig. 3, feature well defined single exothermic crystallization curves. It was observed that the peak temperature of crystallization (T_p) shifted to higher temperature with increasing heating rates (β). T_p decreased with an increase in B_2O_3 content as glass 7A showed the highest T_p value while glass 7-15B showed the lowest T_p among all the investigated glasses. This decrease in T_p with addition of B_2O_3 may be attributed to the decrease in viscosity of the glasses which led to the higher mobility of different ions and ionic complexes operative in crystallization process of the glasses. The addition of SrO slightly decreased the T_p of the glasses (7(Sr)-2B and 7(Sr)-5B) in comparison to BaO-containing glasses (7-2B and 7-5B) (Table 4). A detailed investigation related to the effect of B_2O_3 on the crystallization kinetics of these glasses will be published in another article.

Table 5
Properties of the sintered glass-ceramics produced from glass-powder compacts after heat treatment at different temperatures for 1 h.

Composition	800 °C	850 °C
Shrinkage (%)		
7-2B	16.30 ± 0.28	16.69 ± 0.36
7-5B	17.26 ± 0.34	17.08 ± 0.25
7-10B	16.61 ± 0.31	16.97 ± 0.56
7-15B	8.35 ± 0.15	8.35 ± 0.15
7(Sr)-2B	16.45 ± 0.05	16.80 ± 0.49
7(Sr)-5B	17.20 ± 0.18	17.15 ± 0.46
Density (g cm^{-3})		
7-2B	3.04 ± 0.006	3.15 ± 0.001
7-5B	3.11 ± 0.004	3.09 ± 0.002
7-10B	3.02 ± 0.002	3.00 ± 0.001
7-15B	Samples are highly porous	
7(Sr)-2B	3.01 ± 0.003	3.09 ± 0.001
7(Sr)-5B	3.05 ± 0.001	3.04 ± 0.005

3.2. Crystallization behavior and properties of sintered glass-ceramics

3.2.1. Non-isothermal conditions at 800 and 850 °C (1 h)

In the case of the investigated compositions (Table 2), well-sintered dense glass-powder compacts were obtained after heat treatment at 800 °C for compositions containing B_2O_3 ≤10 wt.%. Sintering preceded crystallization and the appearance of the samples did not change at higher temperatures. There was no evidence of detrimental effects, such as deformation or formation of open porosity, in the temperature interval of 800–850 °C. At a particular temperature, the shrinkage of BaO-containing compositions increased with addition of B_2O_3 content up to 5 wt.% (Table 5). Further addition of B_2O_3 (7-10B and 7-15B) led to a decrease in shrinkage of the GCs, thus, evidencing poor sinterability. The shrinkage of SrO-containing GCs is almost similar to its BaO-containing counterparts. Among all the investigated compositions, 7-5B showed the highest shrinkage (17.26%) after sintering at 800 °C, while the lowest was exhibited by GC 7-15B (8.35%). The shrinkage results indicate that addition of B_2O_3 up to 5 wt.% in the glasses improves the sintering ability of the glass-powder compacts, which will further reduce the porosity of the resultant GCs and improve their mechanical strength.

The evolution of crystalline regime of the glass-powder compacts at 800 and 850 °C (always for 1 h) is demonstrated in the X-ray diffractograms of Fig. 4, while characteristic microstructures (observed by SEM) are shown in Fig. 5. The glass compositions 7A, 7-2B and 7(Sr)-2B were highly amorphous after heat treatment at 800 °C. The addition of 2 wt.% B_2O_3 in 7A (7-2B) led to the initiation of crystallinity in the resultant GC 7-2B, which was confirmed by the existence of very low intensity XRD peaks of augite (designated as Aug; ICDD card: 01-078-1392) (Fig. 4a). However, with further increase in B_2O_3 content and, increase in temperature to 850 °C, Aug precipitated out to be the only crystalline phase in all the resultant GCs (Fig. 4). No boron containing phases were observed for any of the compositions after sintering for 1 h at 800 and 850 °C. However, the intensity of the XRD peaks of the Aug was observed to depend on the B_2O_3 content in the parent glass and was found to be maximum for GC 7-5B at both the temperatures (Fig. 5a). The GCs with B_2O_3 content higher than 5 wt.% showed a considerable decrease in the intensity of the XRD peaks of Aug (Figs. 4 and 5b), with the GCs containing 15 wt.% B_2O_3 showing the lowest intensity (Fig. 5c) among all the investigated compositions, implying towards the stabilization of amorphous phase in the GCs. Similar results have recently been reported by Hillers et al. [26] where they showed that an aluminosilicate E-glass containing 7 wt.% B_2O_3 crystallized slowly in comparison to the glass containing 2 wt.% B_2O_3. They also did not detect any boron containing crystalline phases; however, crystal

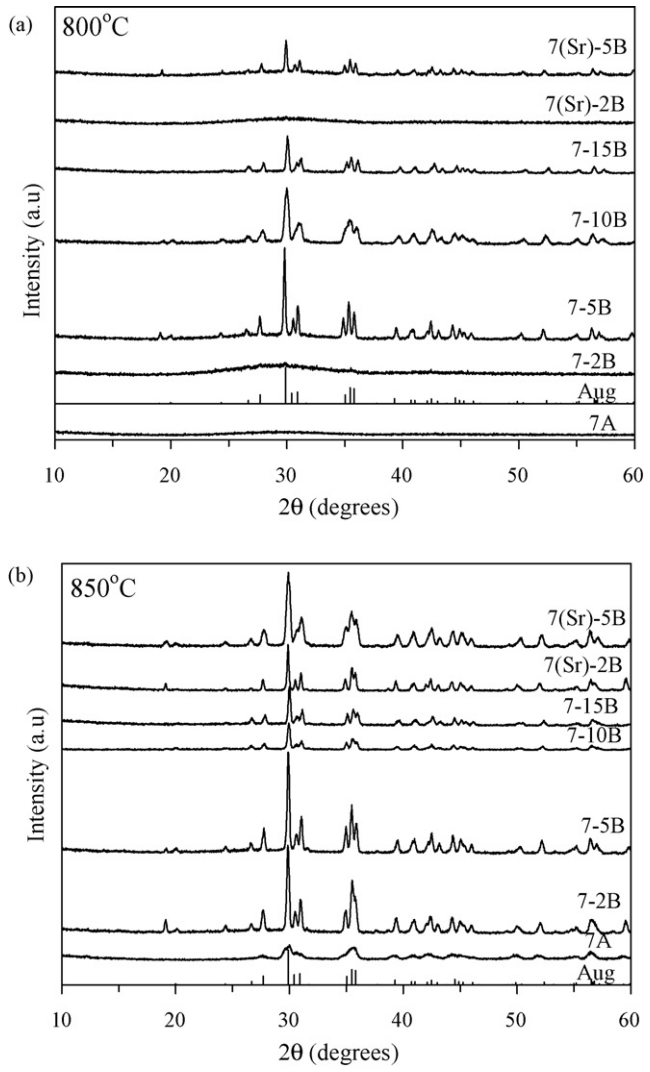

Fig. 4. X-ray diffractograms of glass-powder compacts sintered at (a) 800 °C, (b) 850 °C, for 1 h.

growth rate was significantly decreased with the addition of boron in the glasses [26]. The intensity of the XRD peaks of Aug in GCs 7(Sr)-2B (Fig. 5c) and 7(Sr)-5B (Fig. 5d) were lower in comparison to BaO-containing GCs 7-2B and 7-5B, respectively. This may be explained on the basis of crystallization kinetics studies on the parent glasses, which will be published as another study.

The density of the GCs was considerably affected by the extent of crystallinity in the GCs. With respect to temperature, GC 7-5B showed the highest density among all the investigated GCs after sintering at 800 °C, while GC 7-2B exhibited the highest density among all the GCs sintered at 850 °C (Table 5). The higher density of GC 7-2B at 850 °C and for 7-5B at 800 °C is in accordance with the shrinkage results and may be explained on the basis of increase in the crystallinity in the GCs at a particular temperature, as is evident from the XRD (Fig. 4). We could not measure the density of the GCs from composition 7-15B as these GCs were highly porous in nature. The density of GCs 7(Sr)-2B and 7(Sr)-5B was lower than GCs 7-2B and 7-5B at any particular temperature (Table 5). This may be due to the lower density of SrO in comparison to BaO and lower crystallinity in SrO containing GCs in comparison to BaO-containing GCs, as revealed by XRD (Fig. 4).

The results obtained from density and shrinkage measurements indicate that compositions containing 2 and 5 wt.% B_2O_3 exhibit good sintering ability in comparison to higher B_2O_3 content GCs, which is a desirable result with respect to optimization of GC sealant [1]. Also, as discussed above, glass and GC sealants with high content of B_2O_3 will degrade the seal. Further more, addition of low amount of B_2O_3 in the glass will aid in wetting and flowability properties [27].

Table 6
CTE $\times 10^6$ K^{-1} (200–600 °C) of the glass-ceramics produced at different conditions.

Composition	850 °C, 1 h	800 °C, 300 h
7A	–	9.42
7-2B	9.14	9.34
7-5B	9.57	9.18
7-10B	8.60	–
7-15B	9.06	–
7(Sr)-2B	9.69	8.99
7(Sr)-5B	9.23	8.85

3.2.2. Isothermal conditions (800 °C)

Prolonged heat treatment of GCs (already sintered at 850 °C for 1 h) at 800 °C for 300 h caused a significant variation in the intensities of the Aug phase in the BaO-containing GCs (Fig. 6). The intensity of Aug for GC 7A became almost twice the intensity of the parent GC (sintered at 850 °C for 1 h), while it reduced to half for GC 7-5B after heat treatment at 800 °C for 300 h. No considerable effect on the intensity of Aug in GC 7-2B could be observed after long-term heat treatment. An orthorhombic polymorph of $BaAl_2Si_2O_8$ (designated as OC; ICDD card: 00-012-0726) was formed in BaO-containing GCs. Interestingly, no considerable effect on the intensity of Aug could be observed in SrO-containing GCs after prolonged heat treatment. A boron containing crystalline phase, namely lanthanum boron silicate (designated as $LaBSiO_5$; ICDD card: 00-019-0650) was detected in both 7(Sr)-2B and 7(Sr)-5B GCs. No polymorph of Sr-containing celsian in both the SrO-containing GCs was observed. However, minor peaks for SiO_2 (designated as Q; ICDD card: 01-073-3437) and sillimanite (designated as Al_2SiO_5; ICDD card: 01-083-1562) were detected in GCs 7(Sr)-2B and 7(Sr)-5B, respectively. It is noteworthy that no monoclinic celsian was detected in any of the investigated compositions even after 300 h of heat treatment.

3.2.3. Thermal expansion behavior

The CTE values of the GCs sintered at 850 °C for 1 h and at 800 °C (GCs already sintered at 850 °C for 1 h) for 300 h are presented in Table 6. Among the GCs sintered at 850 °C for 1 h, the highest value of CTE was shown by 7(Sr)-2B (9.69×10^{-6} K^{-1}) while the lowest was shown by GC 7-10B (8.60×10^{-6} K^{-1}). It is noteworthy that the CTE values presented in Table 6 are in the temperature range 200–600 °C, while the SOFC operating temperature is in the range 700–850 °C. The selection of this temperature range 200–600 °C was due to the fact that GCs with B_2O_3 content ≥5 wt.% showed an abnormal thermal expansion behavior in the temperature region 650–750 °C (Fig. 7). Also, it should be mentioned that the change in slope of thermal expansion curve was highly prominent in BaO-containing GCs in comparison to SrO-based GCs. Recently, similar abnormal thermal expansion behavior was observed for the GCs obtained from barium calcium aluminosilicate (BCAS) GC sealant [28]. BCAS GC sealant (contains 10 mol% B_2O_3) is the most extensively investigated sealant and has been seen with alacrity by the SOFC researchers worldwide [1]. The CTE of the BCAS GCs was obtained from room temperature (R.T.) to 550 °C, which is far below the SOFC operating temperature [28] and no results pertaining to such abrupt changes in thermal expansion of GCs were discussed. In our opinion, such abrupt changes in thermal expansion of GCs can cause unwanted stresses in the SOFC stack during its operation. According to Shelby [29], similar deviation of thermal expansion curve from linear behavior can be obtained for a phase separated

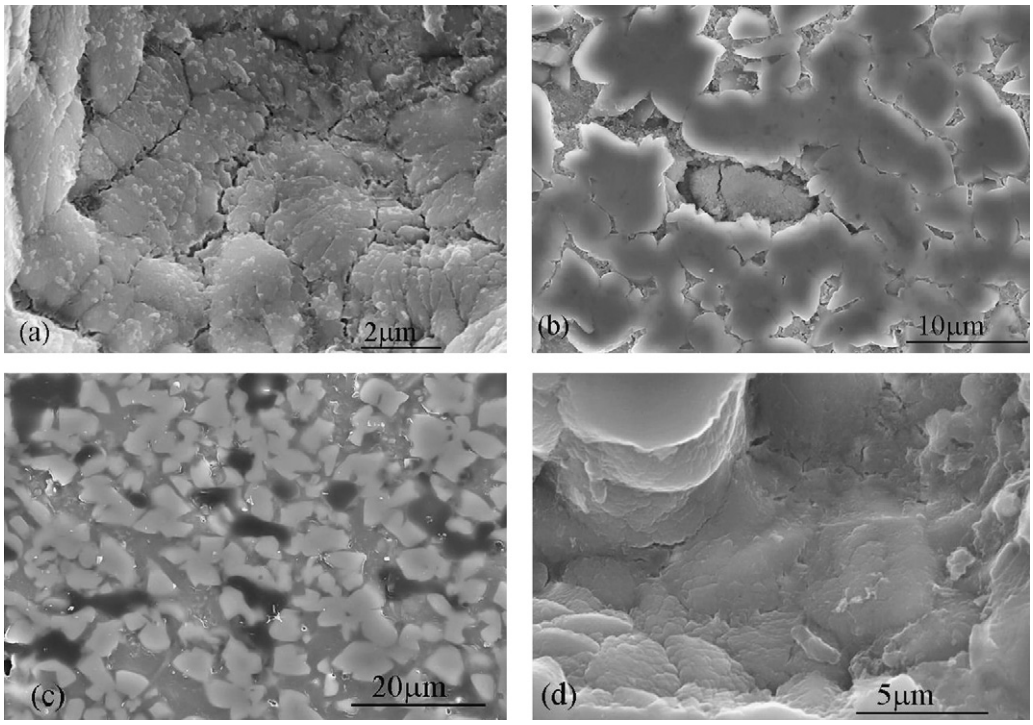

Fig. 5. Microstructure (revealed via SEM imaging after chemical etching of polished surfaces with 2 vol.% HF solution) of the GCs (a) 7-5B heat treated at 850 °C, (b) 7-10B heat treated at 800 °C, (c) 7-15B heat treated at 800 °C and (d) 7(Sr)-2B heat treated at 850 °C for 1 h, respectively.

glass containing two glassy phases, where the more viscous phase is continuous and if the immiscibility temperature for the glass lies above the T_g of the more viscous phase. The thermal expansion curves of this type have been observed for lead borate and barium silicate glasses, where the immiscibility temperature is greater than the T_g of either phase [29]. However, in the present investigation, such behavior has been observed for GCs and not glasses. Therefore, in quest of the reason for the change in the thermal expansion of the GCs in the temperature range 650–750 °C, *in situ* high temperature XRD was performed on the GCs with B_2O_3 content ≥5 wt.%. It is worth to be noted that quartz (designated as Q*, ICDD card: 01-089-8939) precipitated out along with augite in the investigated temperature region in all the GCs (Fig. 7, insert a). As shown in Fig. 1, the investigated glasses show tendency towards phase separation in to SiO_2 and B_2O_3 rich regions at 700 °C. Similar phase separated regions can also be expected in the glassy phase of the GCs, though with different composition in comparison to their parent glasses. This led to the precipitation of quartz from SiO_2 rich glassy phase during heating of the GC (Fig. 7, insert a), consequently, changing the thermal expansion behavior of the GC. However, according to RT-XRD results of the GCs obtained after dilatometry experiments, augite was the only crystalline phase in all the GCs (Fig. 7, insert b). Therefore, it can be suggested that during cooling, the glassy phase in the GC again regained its form, thus leading to the dissolution of previously formed quartz.

We are now in the process of analyzing the expansion behavior of these GCs during cooling and crystalline phase evolution (through *in situ* HT-XRD) after long-term dwells at SOFC operating temperature.

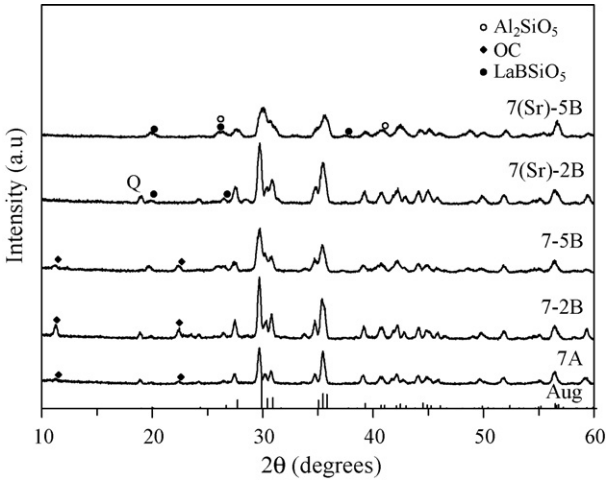

Fig. 6. X-ray diffractograms of sintered GCs (850 °C, 1 h) after heat treatment at 800 °C for 300 h.

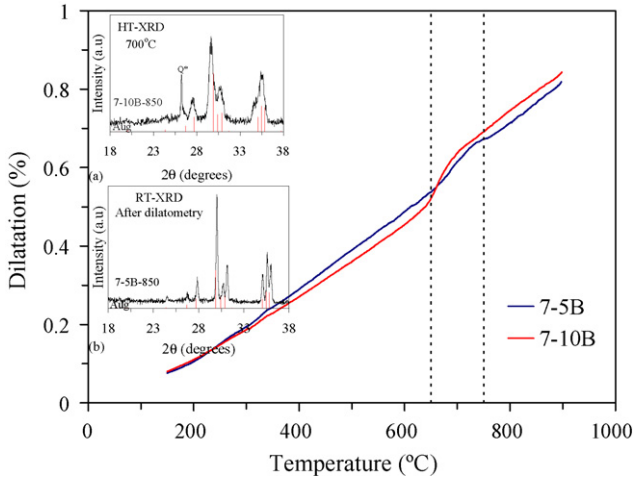

Fig. 7. Thermal expansion curve of GCs 7-5B and 7-10B after sintering and crystallization at 850 °C for 1 h. Inserts: (a) *In situ* HT-XRD for GC 7-10B at 700 °C, (b) XRD for GC 7-5B after dilatometry at room temperature.

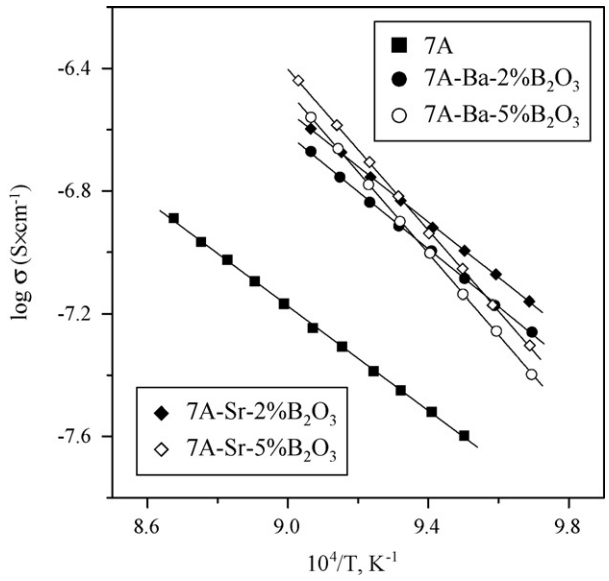

Fig. 8. Total conductivity of dense GCs in air. The data on 7A [5] are shown for comparison. The error bars are smaller than the data point symbols.

The CTE value of SrO-containing GCs decreased considerably after prolonged isothermal heat treatment at 800 °C for 300 h due to the simultaneous presence of different crystalline phases while the CTE of the GC 7-2B slightly increased. Generally, CTE values of 7A, 7-2B and 7-5B match fairly well the CTE of 8YSZ that varies in the range $(9.8–10.4) \times 10^{-6}\,K^{-1}$ at the SOFC operation temperatures.

3.3. Electrical properties and stability of GCs in contact with SOFC components

In the light of the above presented results, it can be concluded that GCs containing B_2O_3 ≤5 wt.% show desirable results with respect to optimization of GC sealant for SOFCs. Therefore, further experimental results will be focused on compositions containing B_2O_3 ≤5 wt.%.

3.3.1. Electrical conductivity of sintered GCs

Small additions of B_2O_3 (2 wt.%) resulted in 3–4 times increase of the total conductivity of dense GCs compared to the boron-free GC (7A) (Fig. 8). Nevertheless, the conductivity is still as low as $(2.1–2.5) \times 10^{-7}\,S\,cm^{-1}$ at 830 °C and $(5.5–6.9) \times 10^{-8}\,S\,cm^{-1}$ at 760 °C. Also, the activation energy (E_A) is similar to that of parent GC, 7A (Table 7), thus indicating that the conduction mechanism remains essentially unchanged. Further increase in the B_2O_3 content up to 5 wt.% does not lead to significant variations of total conductivity in the studied temperature range, but results in substantially higher activation energy. Whatever the mechanisms, the results unambiguously show that the studied GCs can be used as sealants for intermediate-temperature SOFCs operating at temperatures below 780–800 °C. A negligible difference in E_A was observed when BaO was replaced with SrO in the GCs.

Table 7
Activation energy for the total conductivity of glass-ceramics in air.

Glass	T (°C)	E_A (kJ mol^{-1})
7A	780–880	172 ± 3
7-2B	760–830	188 ± 4
7-5B	760–830	263 ± 3
7(Sr)-2B	760–830	182 ± 3
7(Sr)-5B	760–830	261 ± 3

3.3.2. Interfacial adhesion, stability and electrical resistivity in contact with solid electrolyte and interconnect materials

The results of wetting experiments suggest strong interfacial adhesion between the investigated compositions and 8YSZ. In agreement with our previous study [5], good wetting regime was observed (i.e. contact angle <90°) and continuous interfaces, no reaction zones, no cracks or gaps, were revealed after cross sectioning and polishing. No reaction products were also determined by XRD analysis of compact samples made of the powder mixtures of glasses and 8YSZ after heat treatment under the similar conditions (i.e. 850 °C, 1 h and then 800 °C, 300 h).

Two SOFC interconnect alloys, Crofer22 APU and Sanergy HT, were investigated for their chemical compatibility with the investigated glasses. All the sealing GCs bonded well to the metallic interconnects and no gaps were observed even at the edges of the joints. Fig. 9 shows the SEM images of the interface of interconnect/glass joins, respectively, after heat treatment at 850 °C for 1 h, followed by 800 °C for 300 h in air. The extent of diffusion of constituent elements from the alloy interconnects into the glass and vice versa (Fig. 9) has been observed through EDS element mapping and line scanning. As is evident from Fig. 9a, an interaction zone of less than submicron thickness, has been formed at the interface between Crofer22 APU and glass 7-2B. From the element mapping of Cr, Fe and Ba (Fig. 9a) and the elemental line profile of diffusion of elements (Fig. 9b), it is clear that the reaction zone is rich in Ba and Cr and poor in Fe. The concentration of Cr shows an increase at the interface (Fig. 9b) and then decreases considerably, while the relative concentration profile of Ba is approximately constant across the interface suggesting the absence of diffusion barriers for this element. The thickness of the Cr- and Ba-rich reaction zone at the interface between Crofer22 alloy and glass increased with increase in B_2O_3 content to 5 wt.% (Fig. 9b), thus evidencing high reactivity. The EDS element mapping (Fig. 9a and c) revealed that the brown spots visible in the interconnect region above the interface are rich in Ba. It is worth to be noted that the investigated glasses 7-2B and 7-5B contain 2.50 mol% BaO and 4.38 mol% B_2O_3 respectively, while the amount of BaO and B_2O_3 in the barium aluminum silicate (BAS) based and BCAS based glass and GC sealing materials varies between 35–45 mol% and 0–15 mol%, respectively [1]. If, ~2.5 mol% BaO in the presence of 4.38 mol% B_2O_3 can cause such an adverse reaction at the interface of glass/interconnect, then we can definitely expect adverse reaction products for glasses and GCs containing higher amount of BaO and B_2O_3. SrO-containing glasses, 7-2B and 7-5B showed highly stable interface with Crofer22 alloy (Fig. 9d) in comparison to BaO-containing glasses. A good wetting regime and continuous interfaces with minimal reaction zones, no cracks or gaps, were revealed after cross section and polishing. No significant diffusion of Sr into the Crofer22 alloy or formation of Cr-rich reaction product was observed (Fig. 9d and e). This shows that Cr-rich interface was not formed in the absence of BaO. It has been reported earlier that BaO containing glasses interact chemically with chromia-forming alloys forming $BaCrO_4$, which leads to Ba depletion in the GCs and to the separation of GCs from the alloy matrix due to thermal expansion mismatch [30]. In the present investigation, we did not observe any separation of GC from the alloy matrix after 300 h of heat treatment.

In comparison to Crofer22 APU, the investigated GCs showed a better compatibility with Sanergy HT interconnect alloy (Fig. 9f). A thin reaction zone of lower thickness in comparison to that observed with Crofer22 alloy was observed at the interface between glass/Sanergy HT joins. Also, the CTE of Sanergy HT is lower $(11 \times 10^{-6}\,K^{-1})$ than Crofer22 alloy $(11.6 \times 10^{-6}\,K^{-1})$ in the temperature range of 20–700 °C [13,14], which is good for compatibility with GC sealants. Moreover, it was recently reported that higher amount of Si in the metallic interconnect enhances the rate of cor-

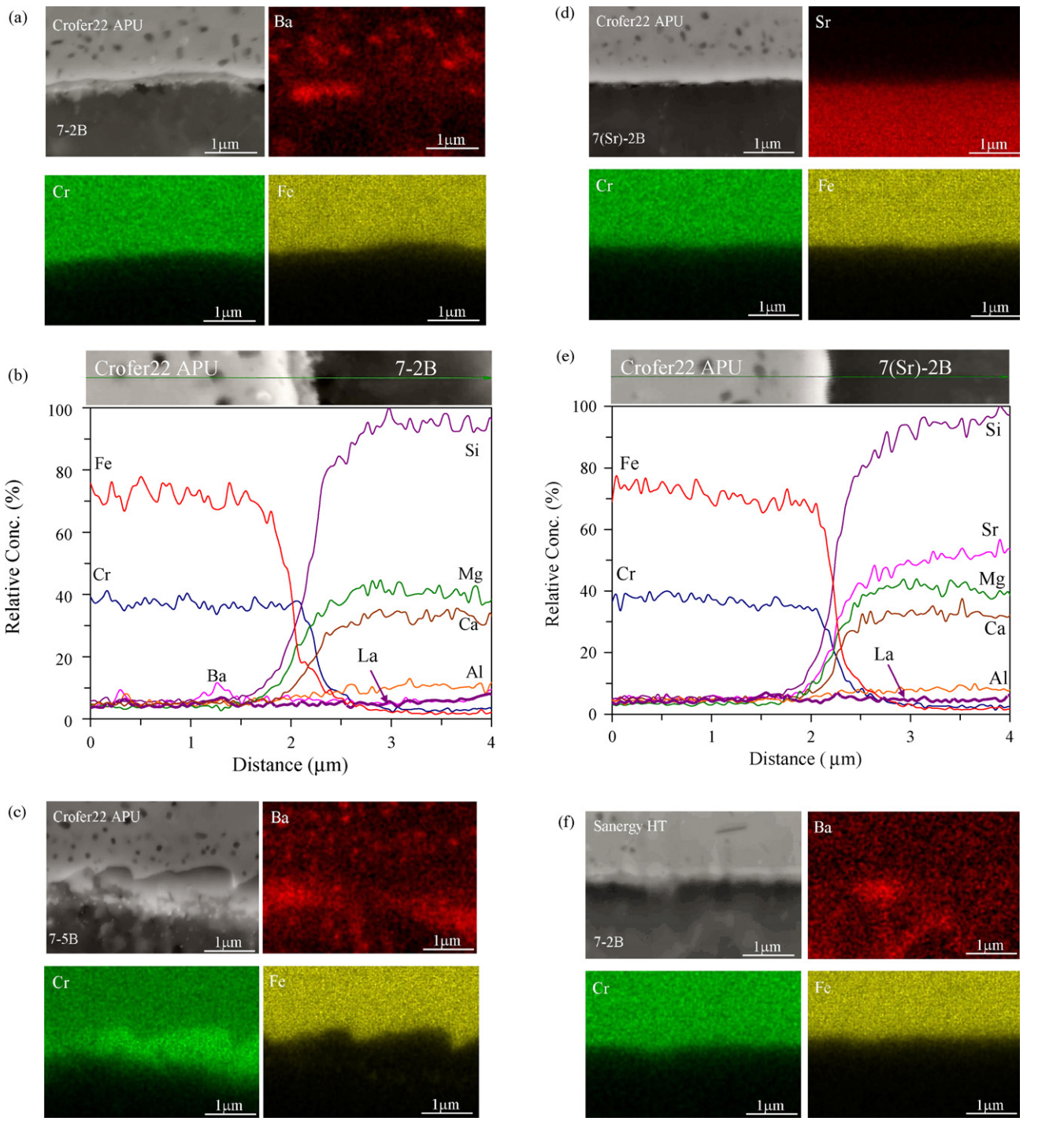

Fig. 9. (a) Microstructure (SEM) and EDS element mapping of Ba, Cr and Fe at the interface between Crofer22 APU/glass 7-2B, (b) EDS line profile for diffusion of various elements from glass 7-2B to Crofer22 APU and vice versa at their interface, (c) microstructure (SEM) and EDS element mapping of Ba, Cr and Fe at the interface between Crofer22 APU/glass 7-5B, (d) microstructure (SEM) and EDS element mapping of Ba, Cr and Fe at the interface between Crofer22 APU/glass 7(Sr)-2B, (e) EDS line profile for diffusion of various elements from glass 7(Sr)-2B to Crofer22 APU and vice versa at their interface, (f) microstructure (SEM) and EDS element mapping of Ba, Cr and Fe at the interface between Sanergy HT/glass 7-2B developed after heat treatment at 850 °C for 1 h and 800 °C for 300 h in air.

rosion attack, leading to the degradation of the SOFC stack [31] and unfortunately, Crofer22 APU alloy contains higher Si content than Sanergy HT (Table 3). Therefore, Sanergy HT seems to be a better candidate as interconnect material in comparison to Crofer22 APU alloy.

In order to confirm good insulating properties of the GCs, the total electrical resistance of a model cell comprising Crofer 22 APU and YSZ plates joined by the 7A GC sealant, was examined by the impedance spectroscopy. The results showed a very high area-specific resistance, 1.7-2.6 MΩ × cm^2 at 850 °C, which tends to slowly increase with time due to surface oxidation of Crofer 22 APU (Fig. 10). This level of resistivity is very appropriate for practical electrochemical applications, such as SOFCs. At the same time, one should note that the total resistance of such cells is considerably higher than expected from the specific conductivities and thicknesses of all components. The latter may indicate formation of thin blocking layers at the interfaces, in particular at the GC| YSZ boundary, invisible by SEM.

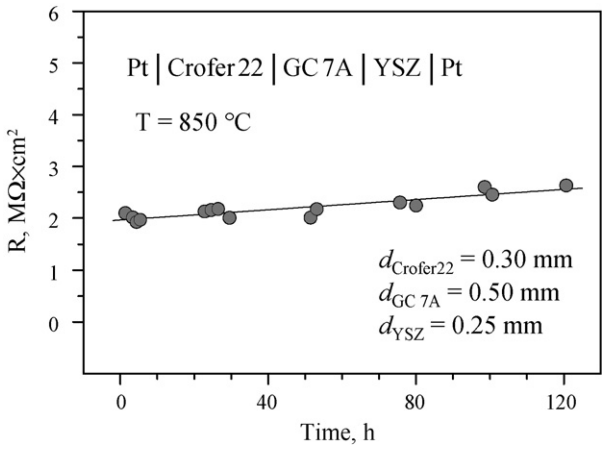

Fig. 10. Total electrical resistance of a model cell comprising Crofer 22 APU and YSZ plates joined by the 7A GC sealant.

The thermal shock tests showed no crack development in the GCs, joining zirconia ceramics, after quenching in air (Fig. 11a). The sealants remained gas-tight, demonstrating an excellent thermal shock resistance and, thus, suitability of the GC sealants for any startup/shutdown protocols in SOFCs. Quenching in more severe conditions, namely in water, resulted in sealants cracking as illustrated by Fig. 11b. Although the mechanical properties of any Si-containing GCs may hardly be enhanced up to the level characteristic of zirconia-based materials, the specific crack-development patterns observed on water quenching suggests a possibility of further sealant optimization, in particular via the incorporation of nano- or submicron-sized crystalline additives such as tetragonal partially-stabilized zirconia (TZP).

4. Summary

A systematic optimization of La_2O_3-containing diopside based GCs have been made in order to qualify them as sealant materials for SOFC applications. The results obtained can be summarized as follows:

(a) The addition of B_2O_3 in the diopside based glasses led to phase separation phenomenon. With varying boron contents in the glasses, the liquid–liquid phase separation mechanism changed between nucleated droplet phase separation and spinodal decomposition. The glass 7-20B featured lack of transparency and stronger tendency for phase separation in comparison with lower B_2O_3-containing glasses.
(b) The investigated glasses showed a steady decrease in density and CTE; and an increase in molar volume and excess volume with increasing B_2O_3 contents. The T_g and T_s decreased with B_2O_3 additions. The CTE of glasses increased while T_g and T_s decreased with replacement of BaO by SrO. The T_p decreased with an increase in B_2O_3 content, while replacement of BaO by SrO caused a slight decrease in T_p.
(c) The introduction of B_2O_3 in the silicate glass network breaks up Q_3 units and favors the formation of Q_2 units. Boron is present in both 3-coordination state (B_3) and four coordination state (B_4) in the glass structure. The decrease in CTE of the glasses with increasing boron contents may be due to the conversion of B_3 into B_4 in the presence of alkaline earth ions.
(d) Mono-mineral augite GCs were obtained after sintering at 800 and 850 °C for 1 h. The crystallinity of GCs increased with B_2O_3 additions up to 5 wt.%, being higher in BaO-containing GCs in comparison to SrO-containing GCs. Furthermore, GCs containing 2 and 5 wt.% B_2O_3 exhibited good sintering ability before the onset of crystallization.
(e) Augite was the main crystalline phase in all the GCs after 300 h of isothermal heat treatment at 800 °C, but the formation of OC as secondary phase was also observed in BaO-containing GCs. However, no Sr-containing celsian phase was observed in SrO-containing GCs. The GCs 7A, 7-2B, 7-5B, 7(Sr)-2B and 7(Sr)-5B showed highly stable crystalline assemblage, with the complete absence of the detrimental monoclinic celsian.
(f) The CTE values of SrO-containing GCs were higher in comparison to their BaO counterparts after heat treatment at 850 °C for 1 h. However, after long-term heat treatment, CTE of the SrO-containing GCs somewhat decreased, while CTE of BaO-containing GCs slightly increased. GCs containing ≥5 wt.% B_2O_3 showed a deviation from the linear thermal expansion curve in the temperature range 650–750 °C, a non-desirable feature for sealants exposed to temperature cycling.
(g) Although the total conductivity of the GCs increased by 3–4 times with a first addition of 2 wt.% B_2O_3 in comparison to the boron-free GC (7A), the values are still lower than other proposed GC sealants. Further increase in the B_2O_3 content to 5 wt.% did not significantly change the total conductivity within the studied temperature range. The E_A was observed to increase from 172 to 263 kJ mol^{-1} with B_2O_3 increasing from 0 to 5 wt.%, while negligible differences in E_A were found upon replacing BaO by SrO in the GCs.
(h) BaO-containing GCs showed severe reactions at the interface between glass/metallic interconnect, and the reaction zone became thicker with increasing B_2O_3 contents. SrO-containing GCs showed highly stable interface between glass/metallic interconnect joins: no significant diffusion of Sr into the interconnect alloy, and the absence of Cr-rich reaction product at interface were observed. The results indicate that SrO-containing GCs can be better alternative for sealant applications in comparison to BaO containing sealants. However, CTE of the SrO-containing GC sealants needs to be somewhat increased.

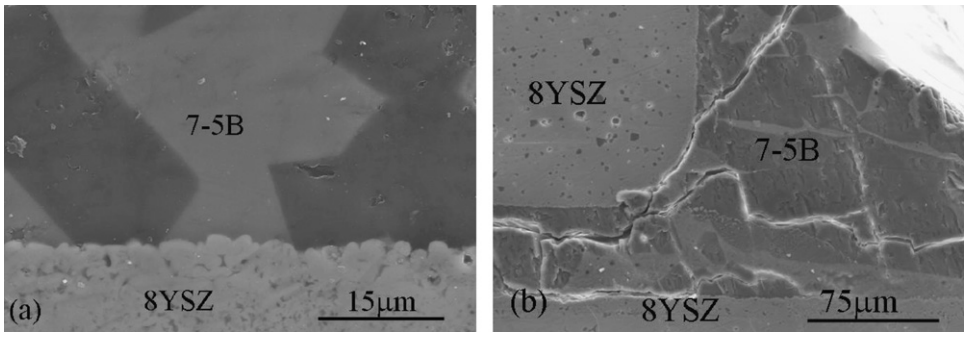

Fig. 11. SEM image of the 8YSZ-GC 7-5B pseudo-cell after thermal shock resistance experiments in (a) air, (b) water, after 15 quenching cycles.

(i) The investigated GCs showed better compatibility with Sanergy HT interconnect alloy in comparison to Crofer22 APU alloy. Also, due to lower CTE and Si content, Sanergy HT seems to be a more suitable interconnect material in comparison to Crofer22 APU for the GCs compositions tested in the present work.
(j) The investigated GC sealants, 7-2B, 7-5B, 7(Sr)-2B and 7(Sr)-5B, demonstrated an excellent thermal shock resistance in air while cracks were only developed on quenching in water. High area-specific resistance, 1.7–2.6 $M\Omega \times cm^2$ at 850 °C was obtained for a model cell comprising Crofer22 APU and YSZ plates joined by the 7A GC sealant. This level of resistivity is very appropriate for practical electrochemical applications, such as SOFCs.

5. Conclusions

From the results presented and discussed in the manuscript, it can be concluded that La_2O_3-BaO-containing diopside based GCs with B_2O_3 content $\leq$5 wt.% exhibited essential features with respect to sealant applications in SOFC namely, good sintering behavior at 800–850 °C, mono-mineral phase composition, absence of detrimental monoclinic celsian phase, long-term CTE stability, good insulating properties, bonding to the metallic interconnects, high area-specific resistance and excellent thermal shock resistance in air. La_2O_3-SrO-containing diopside based GCs, 7(Sr)-2B and 7(Sr)-5B, also exhibited general similar features, but the absence of any severe interface reactions conferred enhanced interface stability to the glass/metallic joins. However, their long-term CTE stability needs to be somewhat improved. Therefore, further experimentation on La_2O_3-diopside based GCs as candidate SOFC sealant materials has to be continued.

Acknowledgements

This study was financially supported by University of Aveiro, CICECO, FCT, Portugal (SFRH/BD/37037/2007) and Swedish Institute, Sweden. Authors are also thankful to Dr. Christopher S. Knee from Gothenburg University, Sweden for his kind assistance in making interaction studies.

References

[1] J.W. Fergus, J. Power Sources 147 (2005) 46.
[2] I.W. Donald, B.L. Metcalfe, L.A. Gerrard, J. Am. Ceram. Soc. 91 (2008) 715.
[3] A. Goel, D.U. Tulyaganov, V.V. Kharton, A.A. Yaremchenko, S. Agathopoulos, J.M.F. Ferreira, J. Am. Ceram. Soc. 90 (2007) 2236.
[4] M.J. Pascual, A. Guillet, A. Durán, J. Power Sources 169 (2007) 40.
[5] A. Goel, D.U. Tulyaganov, V.V. Kharton, A.A. Yaremchenko, J.M.F. Ferreira, Acta Mater. 56 (2008) 3065.
[6] T. Schwickert, R. Sievering, P. Geasee, R. Conradt, Mat.-wiss. u. Werkstofftech. 33 (2002) 363.
[7] S.-B. Sohn, S.-Y. Choi, J. Am. Ceram. Soc. 87 (2004) 254.
[8] P.H. Larsen, F.W. Poulsen, R.W. Berg, J. Non-Cryst. Solids 244 (1999) 16.
[9] K.L. Ley, M. Krumpelt, R. Kumar, J.H. Meiser, I. Bloom, J. Mater. Res. 11 (1996) 1489.
[10] M. Brochu, B.D. Gauntt, R. Shah, G. Miyake, R.E. Loehman, J. Eur. Ceram. Soc. 26 (2006) 3307.
[11] V. Kumar, A. Arora, O.P. Pandey, K. Singh, Int. J. Hydrog. Energy 33 (2008) 434.
[12] M.K. Mahapatra, K. Lu, W.T. Reynolds Jr., J. Power Sources 179 (2008) 106.
[13] Crofer 22 APU, Material data sheet no. 4046, December 2006, Thyssen Krupp VDM, Germany.
[14] Sanergy HT, Material data sheet, Sandvik Materials Technology, Sandvik, Sweden.
[15] W.A. Weyl, "Coloured Glasses," Soc. Glass Technol., 558 (1951) (fifth reprint 1999) ISBN 0-900683-06-X.
[16] J.W. Martin, Concise Encyclopedia of the Structure of Materials, ISBN: 978-0-08-045127-5, Elsevier Science Ltd., UK, 2006.
[17] S.-B. Sohn, S.-Y. Choi, G.-H. Kim, H.-S. Song, G.-D. Kim, J. Non-Cryst. Solids 297 (2002) 103.
[18] R.H. Doremus, Glass Science, 2nd Ed. ISBN: 0-471-89174-6, John Wiley & Sons, Inc., USA, 1994, Chapter 6, p. 103.
[19] M.I. Ojovan, W.E. Lee, An Introduction to Nuclear Waste Immobilisation, (ISBN: 978-0-08-044462-8), Elsevier Science Ltd., UK, 2005, Chapter 17.
[20] D.R. Uhlmann, R.R. Shaw, J. Non-Cryst. Solids 1 (1969) 347.
[21] F. Hamer, J. Hamer, The Potter's Dictionary (ISBN: 0812238109), University of Pennsylvania Press, USA, 2004.
[22] S.-L. Lin, C.-S. Hwang, J. Non-Cryst. Solids 202 (1996) 61.
[23] J.T. Kohli, R.A. Condratr, J.E. Shelby, Phys. Chem. Glasses 34 (1993) 81.
[24] L. Stoch, M. Sroda, J. Mol. Struct. 511–512 (1999) 77.
[25] A.K. Varshneya, Fundamental of Inorganic Glasses (ISBN: 0-12-714970-8), Academic Press Inc., USA, 1994, Chapter 5.
[26] M. Hillers, G. Matzen, E. Véron, M. Dutreilh-Colas, A. Douy, J. Am. Ceram. Soc. 90 (2007) 720.
[27] P.A. Lessing, J. Mater. Sci. 42 (2007) 3465.
[28] K.D. Meinhardt, D.-S. Kim, Y.-S. Chou, K.S. Weil, J. Power Sources 182 (2008) 188.
[29] J.E. Shelby, Introduction to Glass Science and Technology (ISBN: 0-85404-533-3), The Royal Soc. Chem., Cambridge, UK, 1997, Chapter 7.
[30] Z. Yang, J.W. Stevenson, K.D. Meinhardt, Solid State Ionics 160 (2003) 213.
[31] P. Batfalsky, V.A.C. Haanappel, J. Malzbender, N.H. Menzler, V. Shemet, I.C. Vinke, R.W. Steinbrech, J. Power Sources 155 (2006) 128.